# Crystallization Kinetics of an Ethylene Oxide–Propylene Oxide Triblock Copolymer (sym-EPE) in Dilute Solution from the Field-Free Decay of the Electric Birefringence

**Michael Dröscher[1] and Thor L. Smith***

*IBM Research Laboratory, San Jose, California 95193.* *Received February 10, 1981*

ABSTRACT: The field-free decay of the electric birefringence (Kerr effect) was used to determine the growth of single crystals in ethylbenzene containing 2 mg/mL of a PEO–PPO–PEO triblock copolymer, where PEO and PPO denote poly(ethylene oxide) and atactic poly(propylene oxide), respectively. The linear size of the crystals was found to increase in proportion to the square root of time over a substantial portion of the crystallization period at temperatures from 16.5 to 24.4 °C; the solutions were self-seeded at temperatures from 30.1 to 34.0 °C. When the crystallization temperature was increased 6.5 °C, the half-time for crystallization increased 30-fold. The unusual dependence of the size of growing crystals on time has been reported previously only by Kovacs and Manson for the crystallization of a diblock copolymer of atactic polystyrene and PEO from dilute solutions. From optical micrographs of the crystals in three suspensions, we found that the size distribution of the crystals is narrow and that the average size agrees closely (≤2%) with that obtained from the field-free decay of the electric birefringence. Data from SAXS and DSC measurements indicate that the crystal thickness increases significantly with the crystallization temperature and that 15–23% of the units in the PEO segments reside in the amorphous layers on the crystals.

## Introduction

The kinetics of crystallization of polymers in dilute solutions have been studied by using microscopy[2-5] to determine periodically the size of the growing crystals and also by dilatometry[6-9] to obtain the overall rate of crystallization. When the growing crystals are essentially monodisperse, as effected by the so-called self-seeding technique[7,10,11] dilatometric data can be related to crystal size from a knowledge of certain quantities, including the final crystal size and degree of precipitation.[7] Techniques less commonly used to study crystallization kinetics include light scattering to determine the size of submicron crystals,[12] NMR to monitor the decrease in concentration of a dissolved polymer,[4] and infrared spectroscopy to follow the crystallization of isotactic polystyrene in solution.[13]

The size of crystals in a dilute suspension can also be determined by measuring the field-free decay of birefringence, which occurs after an electric pulse has been applied to the suspension. That such suspensions exhibit a strong Kerr electrooptic effect was shown by Picot et al.[14,15] They investigated suspensions of single crystals prepared by self-seeding solutions of a diblock copolymer of poly(ethylene oxide) (PEO) and polystyrene (PS) and also of PEO and polyethylene homopolymers. Thereafter, a detailed investigation[16] was made of the electric birefringence of suspensions of single crystals prepared from solutions of a PEO–PPO–PEO triblock copolymer (Pluronic polyol F127) in ethylbenzene, where PPO denotes atactic poly(propylene oxide).

This paper discusses primarily the growth of crystals from dilute solutions, determined by measuring periodically the field-free decay of the birefringence. Kinetic data at different temperatures were thereby obtained on crystal growth from ethylbenzene solutions of a PEO–PPO–PEO triblock copolymer self-seeded at different temperatures.

When all crystals in a dilute solution of a homopolymer have been nucleated simultaneously, e.g., by self-seeding, the rate of linear growth of the crystals is a constant, except during the latter stage of growth, as is well established.[2-5,12] In contrast, the present data show that the linear dimension of square lamellar crystals from the triblock copolymer increases linearly with the square root of time during a substantial portion of the crystallization period. A similar finding was reported by Kovacs and Manson,[7] who studied comprehensively by dilatometry and optical microscopy the crystallization of a PS–PEO diblock copolymer in ethylbenzene and other solvents. The crystallization kinetics, which were consistent approximately with the Avrami[17] equation, were found to depend considerably on the thermal history of the solution. The exponent $n$ in the Avrami equation was evaluated from the slope of a crystallization isotherm at its inflection point and found to vary from about 1.0 to 1.2 when the self-seeding temperature was 35 °C or lower and the crystallization temperature was between 20 and 30 °C. These values of $n$ indicate that the linear dimension of the crystals increased linearly with $t^{1/2}$, or nearly so, over some range of the crystallization time $t$. As the present findings are similar, it appears that different processes control the crystallization rate of homopolymers and block copolymers containing a noncrystallizable segment. However, as discussed later, the explanation proposed by Kovacs and Manson probably does not account for our results.

## Experimental Section

**Materials.** The PEO–PPO–PEO triblock copolymer (Pluronic polyol F108) was kindly supplied by BASF Wyandotte Corp. According to the BASF Wyandotte literature, its molecular weight is 14 000 and its PEO content is 80 wt %. The latter was also obtained by us from a proton NMR spectrum. It follows from these data that the molecular weights of the inner PPO block and of each outer PEO block are about 2800 and 5600, respectively. $^{13}C$ NMR spectra measured previously[16] on two other Pluronic polyols showed that the PPO blocks are atactic.

In our work, solutions of the triblock copolymer F108 were prepared in freshly distilled ethylbenzene.

The molecular weight distribution, obtained by gel permeation chromatography on seven Pluronic polyols that had been precipitated from dilute benzene solutions by the addition of isooctane, has been reported[18] to be rather narrow (i.e., $M_w/M_n \approx 1.2$). For an unfractionated sample of F108, our GPC data showed that $M_w/M_n$ equals 1.17. Because the number-average molecular weights obtained[18] by vapor-pressure osmometry on the precipitated samples agreed reasonably well with those reported by BASF Wyandotte, it appears that the Pluronic polyols contain little or no material of low molecular weight.

**Preparation and Morphology of Crystals.** To grow crystals by the self-seeding technique,[10,11] a solution containing 2 mg/mL of the triblock copolymer in ethylbenzene was first prepared at 60 °C to ensure complete dissolution. Crystallization was then allowed to occur at room temperature. To conduct an experiment, about 1 mL of the suspension of crystals, which had been at room temperature for 1–2 weeks, was poured into the Kerr cell and

0024-9297/82/2215-0442$01.25/0 

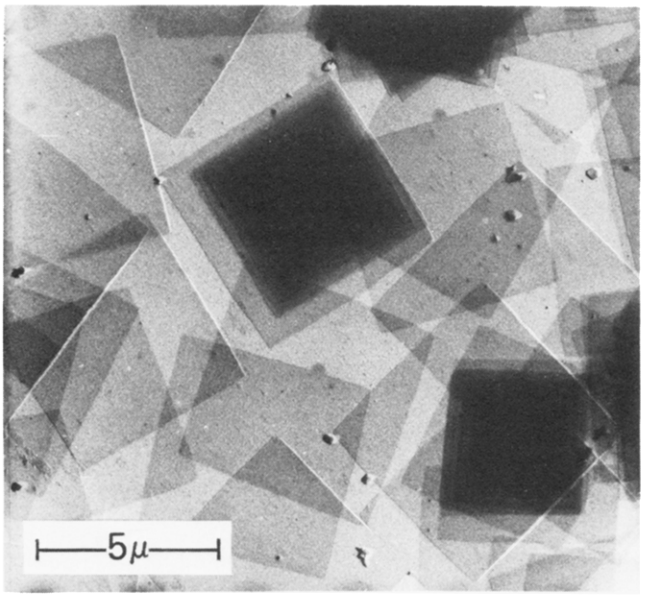


**Figure 1.** Electron micrograph (replica) of crystals grown from a solution of the PEO–PPO–PEO triblock copolymer (2 mg/mL) in ethylbenzene. The seeding and crystallization temperatures were 34.0 and 19.2 °C, respectively.

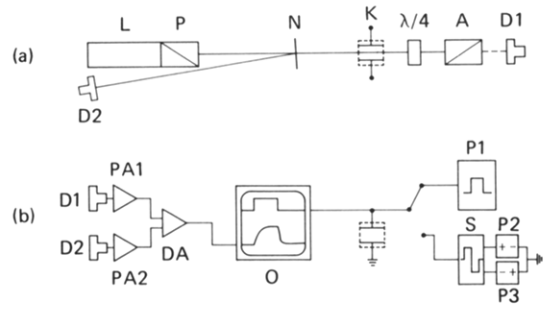


**Figure 2.** Block diagram of birefringence apparatus: (a) and (b) show, respectively, the optical and electrical components.

placed in a constant-temperature bath at a selected seeding temperature, $T_s$, between 30.1 and 34.0 °C for some 20–40 min to obtain a solution that appeared clear. The Kerr cell was next placed in a temperature-controlled jacket mounted in the birefringence apparatus and maintained at a selected crystallization temperature, $T_c$, between 16.5 and 24.4 °C. The fluid in the cell reached a constant temperature in about 4 min. During the ensuing crystallization period, the field-free decay of the birefringence was determined periodically. Both $T_s$ and $T_c$ were controlled to better than 0.1 °C.

Crystals examined by phase-contrast optical microscopy were found to be square lamellae and nearly monodisperse. Figure 1 is an electron micrograph of crystals grown at 19.2 °C after seeding at 34.0 °C. Although the crystals are seemingly fragile, only a few fragments were observed after a suspension had been subjected to a number of electric pulses, required to monitor the birefringence relaxation periodically.

**Birefringence Apparatus.** Techniques for measuring transient birefringence are discussed in a recent monograph[19] and in review articles[20-22] and the references cited therein.

The present apparatus is shown schematically in Figure 2. The light source (L), whose wavelength is 632.8 nm, is a 2-mW helium–neon laser (Oriel Corp.). The laser with the mounted polarizer (P) is arranged such that the electric vector of the light is inclined 45° to the electric field in the Kerr cell (K). The light is partially reflected by a neutral-density filter (N) onto a reference photodiode (D2). The nonreflected light passes through the Kerr cell and then through a 632.8-nm quarter-wave plate whose slow axis is oriented 135° to the electric field. The analyzer (A) is mounted in a precision rotatable holder and is oriented $(135-\alpha)°$ to the electric field, where the angle $\alpha$ was set precisely at a value between −2 and −3°, as discussed subsequently. In the absence of an electric field, light of intensity $I_\alpha$ reaches the photodiode D1.

The Kerr cell is essentially that described elsewhere.[19] It consists of a 10-mm-square Pyrex cuvette, selected such that its strain birefringence is very low. Two platinum electrodes are held 3.5 mm apart by two Teflon spacers, the electrodes and spacers being placed in a machined Teflon piece that also contains the electrical leads. This assembly is placed in the cuvette. The length of the optical path within the cell is 9.5 mm.

Rectangular pulses were generated by P1, which could supply a pulse of preselected duration between 1 and 1000 ms and at a field strength from about 60 to more than 1100 kV/m. The rise and decay times of the pulse were less than 10 and 20 μs, respectively. Longer pulses at field strengths below 30 kV/m could be obtained with the power supply P2 (Hewlett-Packard 6515A) and a manual switch. Though not discussed in this paper, some data, which supplement those reported previously,[16] were obtained by applying a pulse and then reversing its polarity; for this purpose, P2, P3, and the special switch S were used.

During an experiment, the outputs from the photodiodes D1 and D2 (Pin 6, United Detector Technology, Inc.) were passed through preamplifiers (PA1 and PA2) which provided a low-voltage bias on the photodiodes. To eliminate the effect of fluctuations in the intensity of the light, from either room illumination or the laser, the outputs from PA1 and PA2 were subtracted by a differential amplifier (DA). The resulting signal, amplified by a 1A4 plug-in unit, was displayed on a Tektronix 549 dual-beam storage oscilloscope along with the rectangular voltage pulse from P1. Whenever a permanent record was desired, the oscilloscope traces were recorded on Polaroid film. To prevent heating of a sample by the laser beam, the beam shutter was opened only while making a measurement.

**Evaluation of Birefringence.** When the angle between the electric field and the analyzer is $(135-\alpha)°$, as mentioned above, it has been shown[19] that

$$I_\alpha = KI_0 \sin^2 \alpha \tag{1}$$

$$I_\delta = KI_0 \sin^2 (\alpha + \delta/2) \tag{2}$$

where $I_\alpha$ and $I_\delta$ are the intensities of the transmitted light in the absence and presence, respectively, of an electric field, $I_0$ is the intensity of the incident light, $K$ ($\leq 1$) is a factor that accounts for absorption and reflection of light by the optical components, and $\delta$ is the optical retardation of the sample. When expressed in radians, $\delta$ is given by

$$\delta = 2\pi l(n_\parallel - n_\perp)/\lambda \equiv 2\pi l \Delta n/\lambda \tag{3}$$

where $n_\parallel$ and $n_\perp$ are the refractive indices of the sample parallel and perpendicular to the electric field, $l$ is the path length through the sample, $\lambda$ is the wavelength of the light in a vacuum, and $\Delta n$ is the birefringence. Equations 1 and 2 lead to

$$\frac{I_\delta - I_\alpha}{I_\alpha} \equiv \frac{\Delta I_\delta}{I_\alpha} = \frac{\cos 2\alpha - \cos (2\alpha + \delta)}{1 - \cos 2\alpha} \tag{4}$$

The birefringence of suspensions of crystals of PEO chains is negative.[14] When $\delta < 0$ and $\alpha > 0$, $\Delta I_\delta$ is negative and $|\Delta I_\delta/I_\alpha|$ decreases monotonically with a decrease in $|\delta|$ only when $\alpha > |\delta/2|$, as shown by eq 4. To circumvent this restriction and to increase the sensitivity of the apparatus, the analyzer was oriented such that $\alpha$ was between −2 and −3°. When $\alpha < 0$ and $\delta < 0$, $\Delta I_\delta/I_\alpha$ is positive and always decreases with a reduction in $|\delta|$. In the present work, $\alpha$ was measured with a precision rotator to 0.1° or better and was selected to give a convenient value of $\Delta I_\delta$ at steady state under an applied field.

To determine the birefringence-relaxation time of a suspension, and therefrom the size of the crystals, an electric field whose duration was sufficient to give a steady-state birefringence was first applied and then the field was switched off. The resulting signal was observed on the storage screen of the oscilloscope and then recorded on Polaroid film. From a trace that represents birefringence decay, illustrated in Figure 3, quantities proportional to $\Delta I_\delta$ and $I_\alpha$ were read and used along with eq 3 and 4 to calculate the corresponding values of $\Delta n$. Values of $\Delta n/\Delta n_0$ were obtained that decreased with time from unity to about 0.05 or lower, where $\Delta n_0$ is the birefringence when the field was switched off.

The essentially steady-state birefringences shown in Figures 3a and 3b were obtained by applying 57.2 and 15.0 kV/m, re-

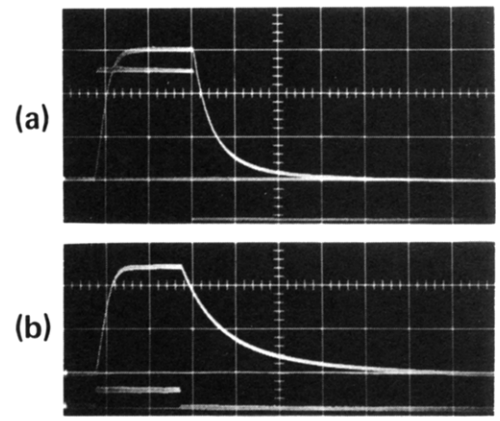


**Figure 3.** Oscilloscope traces from tests on two suspensions of crystals. The rise curves in (a) and (b) represent the response to 57.2 and 15.0 kV/m, respectively. The distances between vertical lines in (a) and (b) correspond to 200 and 1000 ms, respectively, and the decay curves are given by crystals whose respective sizes are 1.38 and 1.94 μm.

Table I
Crystal Sizes Evaluated from Birefringence-Decay Curves and from Optical Micrographs

| quantity | sample no. 24 | 28 | 29 |
|---|---|---|---|
| $T_s$, °C | 31.9 | 32.9 | 30.1 |
| $T_c$, °C | 16.5 | 21.0 | 21.0 |
| $t_c$, min | 395 | 1285 | 1585 |
| $E$, kV/m | 4.0 | 10.0 | 15.4 |
| $-\Delta n_0 \times 10^6$ | 1.80 | 1.87 | 1.51 |
| $\phi_1$ | 0.69 | 0.335 | 0.16 |
| $\tau_1$, s | 1.45 | 1.00 | 0.125 |
| $\phi_2$ | 0.31 | 0.665 | 0.84 |
| $\tau_2$, s | 7.25 | 2.71 | 1.00 |
| $\langle\tau\rangle_B$, s | 3.25 | 2.14 | 0.86 |
| $\langle L^3\rangle_B^{1/3}$, μm | 3.10 | 2.76 | 2.04 |
| $\langle L^3\rangle_{BM}^{1/3}$, μm | 3.06 | 2.75 | 2.00 |
| $\langle L^2\rangle_v^{1/2}$, μm | 2.96 | 2.63 | 1.92 |
| $\langle L^3\rangle_{BM}^{1/3}/\langle L^2\rangle_v^{1/2}$ | 1.03 | 1.05 | 1.04 |

spectively. Analyses of the field-free decay curves by the "peeling" method, discussed subsequently, indicate that the decay curves in (a) and (b) represent average crystal sizes of 1.38 and 1.94 μm, respectively.

To verify that the birefringence could be measured accurately, the Kerr constant[19,20] $B$ ($=\Delta n/\lambda E^2$, where $E$ is the field strength) for nitrobenzene and ethylbenzene, both distilled, was determined at room temperature. The respective values obtained are (4.08 ± 0.2) × $10^{-12}$ and 8.11 × $10^{-15}$ m/V². The corresponding literature values,[23] after converting them to λ = 632.8 nm and from cm/statvolt² to m/V² (the factor is 1.113 × $10^{-7}$), are 4.15 × $10^{-12}$ and 8.39 × $10^{-15}$ m/V², in close agreement with those measured.

In determining a birefringence decay curve, the selected magnitude of the electric field applied to a suspension of crystals depended on the crystal size. When the crystals were small, the applied field was commonly 572 kV/m or higher but was usually between 4 and 30 kV/m when the crystals were large. Representative values of $E$ and $\Delta n_0$ for suspensions of large crystals are included in Table I.

No account was taken of the birefringence of ethylbenzene; its magnitude was negligible compared with that of the crystals when the crystals were very small and at low concentration. For example, $\Delta n$ for ethylbenzene at 1144 kV/m is only 6.7 × $10^{-9}$, and for relatively large crystals it was often greater than −2 × $10^{-6}$ even when the applied field was less than 10 kV/m. More importantly, the birefringence of ethylbenzene decays almost instantaneously and thus it cannot affect the shape of a decay curve resulting from the disorientation of crystals.

## Results

**Size of Crystals from the Birefringence-Relaxation Time.** When a suspension of monodisperse rigid particles is sufficiently dilute so that the hydrodynamic interaction between particles is negligible, the field-free decay of the birefringence, following the application of an electric pulse, is given by[19-21]

$$\Delta n/\Delta n_0 = e^{-t/\tau} \equiv e^{-6\theta t} \tag{5}$$

where $\tau$ is the birefringence-relaxation time and $\theta$ ($=1/6\tau$) is the rotary diffusion coefficient of a particle.

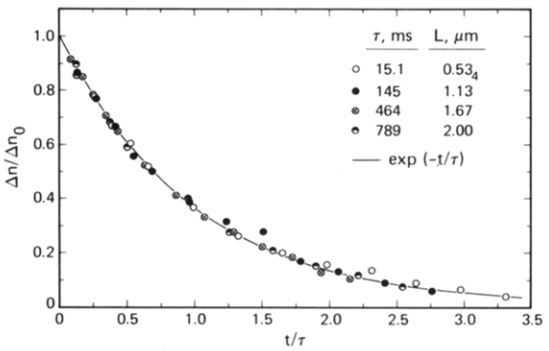


**Figure 4.** Field-free decay of the birefringence shown by a plot of $\Delta n/\Delta n_0$ vs. $t/\tau$, where $\Delta n_0$ is the birefringence when the electric field was removed at zero time and $\tau$ is the birefringence-relaxation time. Measurements were made during the growth of crystals at 22.5 °C from an ethylbenzene solution of the triblock copolymer (2 mg/mL) that had been seeded at 31.9 °C. The tabulated values of $L$ were obtained from $\tau$ using eq 6.

In many instances, decay curves could be represented quite accurately by eq 5, as illustrated by Figure 4. These data were determined at four different times during the growth of crystals at 22.5 °C in an ethylbenzene solution of the triblock copolymer that had been seeded at 31.9 °C. The listed values of $\tau$ in Figure 4 were obtained from the slopes of plots of log $\Delta n$ vs. $t$.

As discussed previously,[16] $\tau$ is related to the length $L$ of a side of a square lamellar crystal by

$$L = [9kT\tau/(4)(2^{1/2})\eta]^{1/3} \tag{6}$$

where $kT$ is the product of the Boltzmann constant and the absolute temperature and $\eta$ is the viscosity of the liquid medium. This equation was derived[16] by considering that the rotary diffusion coefficient of a crystal equals that of a highly oblate ellipsoid whose volume equals that of the crystal and whose equivalent (transverse) axes have the same length as the diagonals of the crystal (i.e., $2^{1/2}L$). No account is taken of the slight reduction in the rotary diffusion coefficient undoubtedly caused by the sheath of noncrystallized segments attached to each face of a crystal.

The values of $L$ listed in Figure 4 were obtained from eq 6 and the values of $\tau$. The viscosity of ethylbenzene is given by[24] $\eta = 8.745 \times 10^{-4}/(1 + 0.01448t + 4.530 \times 10^{-5}t^2)$, where here $t$ denotes the temperature in °C and $\eta$ is the viscosity in Pa·s.

**Distribution of Crystal Sizes.** Consider a dilute suspension of polydisperse rigid particles. If the optical anisotropy factor for each particle is the same and if all particles become fully oriented under an applied electric field, then the subsequent field-free birefringence-decay curve is given by[25]

$$\Delta n/\Delta n_0 = \sum \phi_i e^{-t/\tau_i} \tag{7}$$

where $\phi_i$ is the volume fraction of the $i$th particles, each of size $L_i$, whose birefringence-relaxation time is $\tau_i$. An average relaxation time is defined by[19,26]

$$\int_0^\infty (\Delta n/\Delta n_0)\, dt \equiv \langle\tau\rangle_B = \sum \phi_i \tau_i \tag{8}$$

Whenever an experimental decay curve in the present study was not exponential, the deviation therefrom was

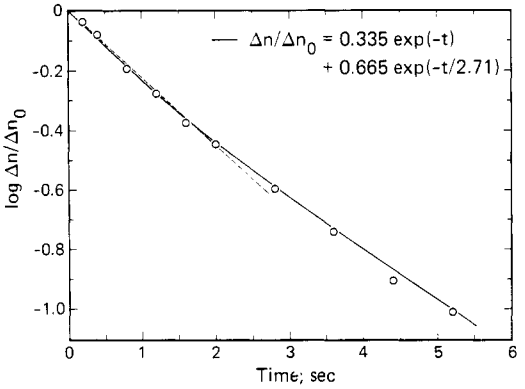


**Figure 5.** Field-free decay of the birefringence shown by a plot of log $(\Delta n/\Delta n_0)$ vs. time, where $\Delta n_0$ is the birefringence when the field was removed at zero time. The circles and the curve represent, respectively, the experimental data and the equation given in the figure. The experimental conditions are given in Table I under sample 28.

small and the curve could be represented by eq 7 containing two exponential terms. The "peeling" method[19,27] was adopted to obtain the four requisite parameters, evaluated by a computer routine. Figure 5, which shows data on sample 28 (Table I), provides an example. The curve represents eq 7 containing the values of $\phi_1$, $\tau_1$, $\phi_2$, and $\tau_2$ given in Table I. As shown below, $\langle\tau\rangle_B$ obtaining from these parameters gives accurately an average crystal size. The parameters individually have no particular physical significance because the crystals had a distribution of sizes, albeit narrow. Furthermore, because the applied field was not always sufficient to orient all particles fully, $\langle\tau\rangle_B$ could depend somewhat on the field strength, in theory, and hence eq 7 and 8 might not be strictly applicable. However, several experiments made with different field strengths showed that the normalized decay curves ($\Delta n/\Delta n_0$ vs. $t$) were independent of the field strength.

Furthermore, according to theory, use of eq 7 and 8 introduces an inconsequential error because the field applied in conducting all experiments was sufficiently high so that $\Delta n_{i,0}/\Delta n_{i,s} > 0.6$ for all crystals, where $\Delta n_{i,0}$ and $\Delta n_{i,s}$ are the steady-state birefringences of the $i$th crystals when under the field and when fully oriented, respectively. In light of previous results,[16] it may be assumed that $\Delta n_{i,0}/\Delta n_{i,s} \cong (1 - 3kT/2.5 \times 10^{-11} L_i^3 E^2)$. Based on this relation and the fact that $\Delta n_{i,0}/\Delta n_{i,s} > 0.6$, it can be shown that $\langle\tau\rangle_B$ derived from a decay curve when $\Delta n_{i,0} \neq \Delta n_{i,s}$ for all crystals should deviate by less than 12%, and usually by a much smaller amount, from the true value of $\langle\tau\rangle_B$, which is independent of the strength of the applied field. Because $\langle L^3\rangle_B^{1/3} \propto \langle\tau\rangle_B^{1/3}$ (see below), the maximum error in $\langle L^3\rangle_B^{1/3}$ should always be less than 4%.

If $n_i$ is the number of crystals of size $L_i$, each having the same thickness, then

$$\langle L^2\rangle_v^{1/2} = (\sum^N n_i L_i^2/N)^{1/2} \quad (9)$$

where $\langle L^2\rangle_v^{1/2}$ is the length of a square crystal whose volume is the number-average volume of all crystals and $N$ is the total number of crystals. Because the volume fraction of the $i$th crystals equals $n_i L_i^2/N\langle L^2\rangle_v$ and $L_i \propto \tau_i^{1/3}$ (cf. eq 6), it follows from eq 8 that

$$\langle L^3\rangle_B^{1/3} = (\sum n_i L_i^5/N\langle L^2\rangle_v)^{1/3} \quad (10)$$

where $\langle L^3\rangle_B^{1/3}$ is the average length of an ensemble of crystals that is proportional to $\langle\tau\rangle_B^{1/3}$.

To determine whether eq 6 and $\langle\tau\rangle_B$ evaluated from a decay curve give the correct value of $\langle L^3\rangle_B^{1/3}$, the size of

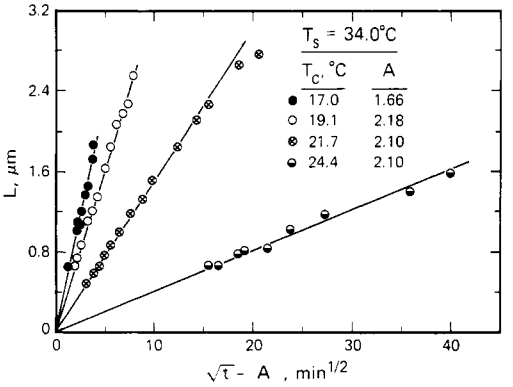


**Figure 6.** Plots showing the dependence of the linear size of crystals on $t^{1/2} - A$, where values of $A$ $(=t_0^{1/2})$ are from Table II.

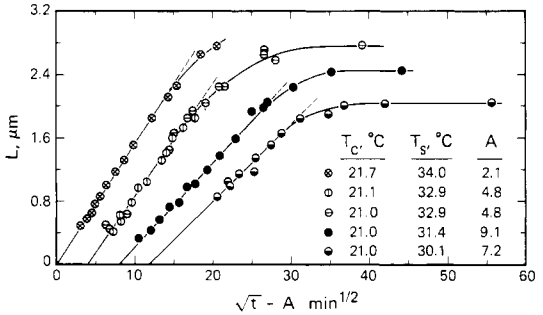


**Figure 7.** Plots showing the dependence of the linear size of crystals on $t^{1/2} - A$. Here, $A$ equals $t_0^{1/2} - B$, where $B$ is a constant to displace the curves for clarity. Values of $t_0$ are from Table II; when $t_0 < 0$, $t_0^{1/2} = -|t_0|^{1/2}$ by definition. Data from duplicate experiments when $T_s = 32.9$ °C are shown.

60–100 crystals in each of three suspensions was measured on optical micrographs. Included in Table I are the temperatures ($T_s$) at which the suspensions were seeded, the crystallization temperatures and times ($T_c$ and $t_c$), and the values of $\phi_i$ and $\tau_i$ ($i = 1, 2$), obtained from decay curves, along with $\langle\tau\rangle_B$. Table I shows that the values of $\langle L^3\rangle_B^{1/3}$ obtained from $\langle\tau\rangle_B$ are only slightly larger (≤2%) than those, $\langle L^3\rangle_{BM}^{1/3}$, calculated from the measured sizes of the crystals according to eq 10. Although the small differences are probably within the experimental uncertainty, it is tempting to propose that all values of $\langle\tau\rangle_B$ from decay curves (and also of $\tau$ for monodisperse crystals) are large by, say, 4%. Such is quite reasonable because, as mentioned before, eq 6 does not account for the hydrodynamic interaction of the noncrystallized chain segments with the solvent. Be that as it may, the present data show that the crystal size derived from a decay curve is reliable and that the polydispersity of crystals is small indeed, as indicated by $\langle L^3\rangle_{BM}^{1/3}/\langle L^2\rangle_v^{1/2}$ (Table I), where $\langle L^2\rangle_v^{1/2}$ was evaluated from values of $L_i$ measured directly.

**Rate of Crystal Growth.** During a substantial fraction of a crystallization period, the size of the crystals increased according to

$$L = k(t^{1/2} - t_0^{1/2}) \quad (11)$$

where $k$ and $t_0$ are constants. Illustrative data are shown in Figures 6–8. (In these figures and the discussion hereafter, $\langle L^3\rangle_B^{1/3}$ is denoted by $L$ for convenience.) Included in Table II are the values of $k$ $(=dL/dt^{1/2})$ and $t_0$ obtained from Figures 6–8 and similar plots of other data. While $t_0^{1/2}$ was usually positive, as expected, it was negative in several instances; then, $t_0$ equals $-(t_0^{1/2})^2$ by definition.

The curves in Figure 7 show clearly how $L$ approaches its final value, $L_\infty$. These values and those from other experiments continued until crystal growth ceased are

Table II
Crystallization Rates and Other Data from Plots of $L$ vs. $t^{1/2}$

| $T_s$, °C | $T_c$, °C | $t_0$, min | $k$,[a] μm/min$^{1/2}$ | $L_\infty$, μm | $(L_{min}{}^b/L_\infty)^2$ | $(L_d{}^c/L_\infty)^2$ |
|---|---|---|---|---|---|---|
| 34.0 | 17.0 | 2.76 | 0.460 | | | |
| | 19.1 | 4.75 | 0.324 | | | |
| | 21.7 | 4.41 | 0.152 | | | |
| | 24.4 | 4.41 | 0.041 | | | |
| 32.9 | 17.5 | 3.80 | 0.381 | | | |
| | 19.4 | 1.82 | 0.286 | | | |
| | 21.1 | 0.64 | 0.141 | 2.76 | 0.024 | 0.59 |
| | 23.8 | −0.42 | 0.0673 | | | |
| 32.2 | 22.8 | 0.49 | 0.0836 | | | |
| 31.9 | 16.5 | 4.62 | 0.533 | 3.20 | 0.018 | 0.56 |
| | 17.6 | 3.35 | 0.425[d] | 3.00 | 0.023 | 0.64 |
| | 19.7 | 2.10 | 0.204 | | | |
| | 21.0 | 14.14 | 0.166 | 2.75 | 0.021 | 0.70 |
| | 22.5 | −1.00 | 0.0744 | 2.05 | 0.069 | 0.69 |
| | 23.0 | −6.25 | 0.0576 | 1.86 | 0.081 | |
| 31.4 | 21.0 | 1.56 | 0.107 | 2.45 | 0.019 | 0.67 |
| 30.1 | 21.0 | −23.0 | 0.0985 | 2.04 | 0.174 | 0.69 |

[a] $k = dL/dt^{1/2}$ during the period that the data fit eq 11. [b] $L_{min}$ is the smallest value of $L$ measured reliably. [c] When $L > L_d$, $dL/dt^{1/2}$ decreases progressively with time. [d] Average of two determinations.

Table III
Crystalline Fraction and Thickness of Crystals[a]

| sample no. | $T_s$, °C | $T_c$, °C | LP, nm | $\Delta H_s$, J/g | $w_c$ | $v_c$ | $h_c$, nm | $S$ |
|---|---|---|---|---|---|---|---|---|
| 1 | 34.0 | 17.2 | 10.7 | 119 | 0.623 | 0.586 | 6.27 | 4.4 |
| 2 | 32.0 | 20.2 | 12.1 | 128 | 0.670 | 0.633 | 7.66 | 3.8 |
| 3 | 34.0 | 21.2 | 12.2 | 122 | 0.639 | 0.602 | 7.34 | 3.8 |
| 4 | 34.0 | 24.1 | 13.2 | 117 | 0.613 | 0.576 | 7.60 | 3.5 |
| 5 | 34.0 | 26.0 | 14.6 | 130 | 0.681 | 0.644 | 9.39 | 3.2 |

[a] LP is the long period, $w_c$ and $v_c$ are the weight and volume fractions of the crystalline portion of a precipitated sample, $h_c$ is the thickness of a crystal, and $S$ is the average number of stems in a crystal from each PEO segment.

included in Table II. The final degree of precipitation was not determined. However, because Lotz and co-workers[28,29] have found that the final degree of precipitation, from ethylbenzene, of a PS–PEO diblock copolymer containing 28% PS was 97%, it is likely that essentially all of our triblock copolymer had precipitated when $L$ reached its terminal value $L_\infty$.

The fraction of precipitated material, $v_p$, at any time during the crystallization process equals $(L/L_\infty)^2$, provided the number of growing crystals remains constant. To show the range of $v_p$ within which $k$ was evaluated from $L$, the minimum crystal size, $L_{min}$, and also the crystal size, $L_d$, at which some deviation from eq 11 was clearly evident were noted. As shown in Table II, $(L_d/L_\infty)^2$ ranges from 0.56 to 0.70, the corresponding values of $L_d/L_\infty$ being 0.75 and 0.84. The values of $(L_{min}/L_\infty)^2$ range from 0.018 to 0.081, the last entry in Table II being overlooked; the corresponding values of $L_{min}/L_\infty$ are 0.13 and 0.28.

An appropriate measure of the crystallization rate is $(L_\infty/k)^2$, which is the time (hypothetical) at which $L$ would equal $L_\infty$ if $L = kt^{1/2}$ for $0 < L \leq L_\infty$. As $L = kt^{1/2}$ for values of $L/L_\infty$ in excess of 0.50 (see Table II), it follows that $t_{1/2} = 0.50(L_\infty/k)^2$, where $t_{1/2}$ is the half-time for crystallization, i.e., the time at which $(L/L_\infty)^2 = 0.50$. This definition of $t_{1/2}$ results from considering that $L = kt^{1/2}$ as $t$ approaches zero. Such is not true because, among other things, the values of $t_0$ (Table II) are not zero. However, if another relation is selected to represent crystal growth, i.e., the Avrami[17] equation, then $t_{1/2} = K(L_\infty/k)^{1/2}$, where $K$ is a constant obtained from the selected relation. The temperature dependence of $t_{1/2}$ is discussed subsequently. (It is worth noting that the Avrami equation can represent the growth of crystals from dilute solution over the entire range of crystallization, even though crystal growth is clearly not impeded by impingement, as shown by Mandelkern and co-workers.[8])

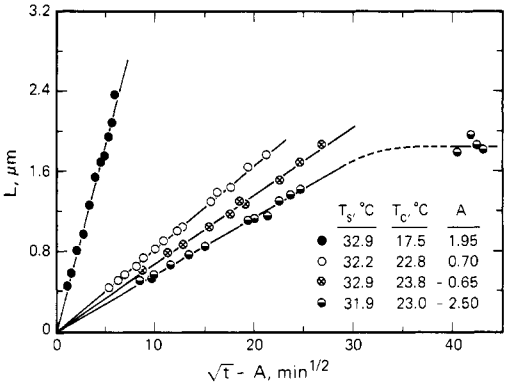


**Figure 8.** Plots showing the dependence of the linear size of crystals on $t^{1/2} - A$, where the values of $A$ ($=t_0{}^{1/2}$) are from Table II; when $t_0 < 0$, $t_0{}^{1/2} = -|t_0|^{1/2}$ by definition.

**Thickness and Amorphous Content of Crystals.** Crystals were grown at five temperatures from 17.2 to 26.0 °C from solutions of the PEO–PPO–PEO block copolymer seeded at 34.0 °C and, in one instance, at 32.0 °C. (The growth rates of the crystals were not determined.) On each batch of crystals, the long period (LP) was determined from small-angle X-ray scattering, and the heat of fusion $\Delta H_s$ was obtained from DSC data measured at a heating rate of 10 °C/min. These data are included in Table III. Some days later, duplicate measurements of $\Delta H_s$ gave values that differed by no more than ±3% from those obtained earlier. (These measurements were made by one of us (M.D.) in the Institut für Makromolekulare Chemie, Freiburg, West Germany.)

For each batch of crystals, the melting peak in the DSC curve occurred at about 59 °C, and melting was complete at 61–62 °C. Booth and Dodgson[18] determined the melting points of crystals in seven undiluted PEO–PPO–PEO triblock copolymers (Pluronic polyols) and reported a melting point of 60 °C for the copolymer whose composition and molecular weight were the same as for our material. For a PEO homopolymer whose molecular weight (5600) equals that of a PEO segment in our triblock copolymer, the reported[18] melting point is 64 °C. (The thermodynamic melting point of crystalline PEO is 69 °C.[30]) For our crystals formed at 17.2 °C, the DSC curve showed a secondary melting peak at 51 °C. With a progressive increase in $T_c$, the secondary peak shifted to a higher temperature and eventually merged with the primary peak. Such secondary peaks have been observed during the heating of bulk-crystallized samples of PEO–PPO–PEO[18] and PPO–PEO–PPO[31] triblock copolymers and also PEO homopolymers.[30,32]

The weight fraction $w_c$ (Table III) of the crystalline PEO in each precipitated sample was obtained from $\Delta H_s/\Delta H_f$, where $\Delta H_f$ is the heat of fusion of PEO crystals, here equated to 191 J/g. (Values of $\Delta H_f$ used in analyzing data on PEO–PPO diblock copolymers[33] and on PEO homopolymers,[34] all of relatively low molecular weight, are 191 and 195 J/g, respectively. The latter was obtained from the stated value[34] ($2.4 \times 10^9$ ergs/cm$^3$) by considering that the density of PEO crystals[35] at 25 °C is 1.23 g/cm$^3$.) The volume fraction $v_c$ of crystalline PEO in each precipitated sample was computed from $w_c$ by considering the densities (g/cm$^3$) at 25 °C of PEO crystals,[35] amorphous PEO,[36] and amorphous PPO[37] to be 1.23, 1.12, and 1.00, respectively. Table III shows that $v_c$ is about 0.61 ± 0.03 and thus the degree of crystallinity depends only slightly, if at all, on the crystallization temperature.

The fraction of the PEO that is amorphous ($w_c/0.8$) is 0.15–0.23. These values are somewhat similar to that found by Mandelkern and associates[38] for crystals, grown in dilute solution at 80 °C, of polyethylene whose molecular weight was 4900. They found that LP and LP − $h_c$ are 13.5 and 2.0 nm, respectively, and hence 15% of the units are amorphous.

Because the crystals were essentially monodisperse, the length of the PEO stems in a crystal is given by $h_c = v_c(\mathrm{LP})$ (Table III) and the number of monomeric units in each stem equals $h_c/0.276$, where 0.276 nm is the reported[39] length of a monomeric unit. The number of stems $S$ (Table III) from each PEO chain equals $(5600/44)(w_c/0.8)/(h_c/0.276)$. As $S$ varies from 4.4 to 3.2, a PEO chain is folded from two to three or four times, depending on the crystallization temperature. The folds must be quite loose, however, because 15–23% of the PEO is amorphous, as mentioned above.

**Concentration of Nuclei.** It might seem that the number of growing crystals would depend only on the seeding temperature. If so, and if all of the dissolved polymer (2 mg/mL) had precipitated when the crystals reached their final size $L_\infty$, the number of nuclei per cm$^3$ is given by $N = 0.002/[\rho(\mathrm{LP})L_\infty^2]$, where $\rho$ (=1.16 g/cm$^3$) is a representative density of the precipitated units, calculated from the data in Table III and the densities of amorphous and crystalline PEO and amorphous PPO, given above. In computing the values of $N$ in Table IV, the requisite values of LP were obtained from a plot of LP against $T_c$, prepared from the data in Table III.

Table IV shows that $N$ increases with a decrease in $T_s$, as expected, when the crystallization temperature was 21 °C. But when $T_s$ was 31.9 °C, $N$ increases significantly with the crystallization temperature, a reflection of the complex nature of the seeding process, illustrated by previous investigations. In studying the seeding of polyethylene solutions, Blundell and Keller[11] found that the final crystal size usually increased significantly with a reduction in $T_c$ (typically, a 25% increase with a decrease in $T_c$ by 5 °C), as also shown by our data in Table IV, even though the same crystal suspension had been seeded in the same way. They also found that the concentration of nuclei depends on both the rate at which a crystal suspension is heated to $T_s$ and the time at $T_s$. Kovacs and Manson[7] found that $N$ depends on both the original crystallization temperature and the time that the crystals remained at this temperature.

Table IV
Calculated Values of Concentration of Nuclei

| $T_s$, °C | $T_c$, °C | $L_\infty$, μm | LP,[a] nm | $N \times 10^{-10}$, cm$^{-3}$ |
|---|---|---|---|---|
| 32.9 | 21.1 | 2.76 | 12.2 | 1.86 |
| 31.9 | 21.0 | 2.75 | 12.2 | 1.87 |
| 31.4 | 21.0 | 2.45 | 12.2 | 2.35 |
| 30.1 | 21.0 | 2.04 | 12.2 | 3.40 |
| 31.9 | 16.5 | 3.20 | 10.2 | 1.65 |
| 31.9 | 17.6 | 3.00 | 10.9 | 1.76 |
| 31.9 | 21.0 | 2.75 | 12.2 | 1.87 |
| 31.9 | 22.5 | 2.05 | 12.5 | 3.28 |
| 31.9 | 23.0 | 1.86 | 12.7 | 3.92 |

[a] Interpolated values of the long period (Table III), based on the assumption that LP depends only on $T_c$.

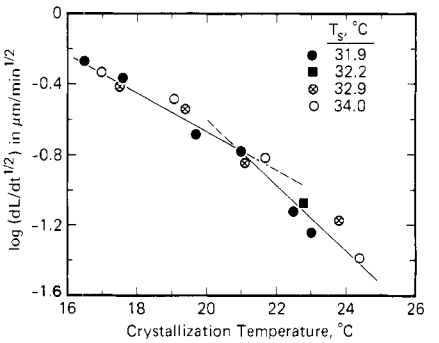


**Figure 9.** Semilogarithmic plot of $dL/dt^{1/2}$ against the crystallization temperature.

**Temperature Dependence of Crystallization Rate.** Although the observed linear dependence of $L$ on $t^{1/2}$ might suggest a diffusion process, such a process clearly does not control the crystallization rate. As shown in Figure 9, $dL/dt^{1/2}$ (=$k$) increases tenfold when the crystallization temperature is reduced from 24.4 to 16.5 °C. (Quite probably, $d[\log (dL/dt^{1/2})]/dT_c$ varies continuously with $T_c$ and not discontinuously as suggested by the lines in the figure.) If $dL/dt^{1/2}$ depends on $L_\infty$, an appropriate measure of the growth rate of crystals is $t_{1/2}$, whose temperature dependence can be considered in terms of nucleation theory.

If the rate of crystal growth is controlled by the frequency at which secondary nuclei form on the edge of a growing crystal, then according to the theory[40] commonly used

$$\log t_{1/2} = BT_d^0/T_c(T_d^0 - T_c) + \log A \qquad (12)$$

where $T_d^0$ is the dissolution temperature of infinitely large crystals, $B$ is a constant that depends on the heat of solution and on the lateral and fold surface energies, and $A$

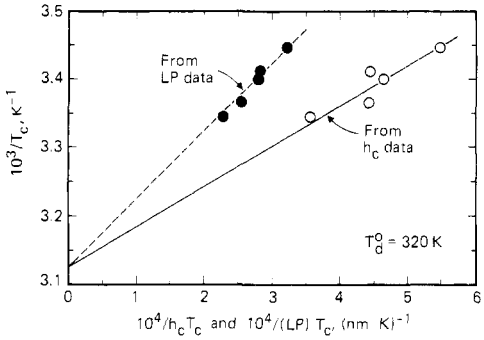


**Figure 10.** Plot of data according to eq 13 to estimate $T_d^0$. Values of the long period are also shown.

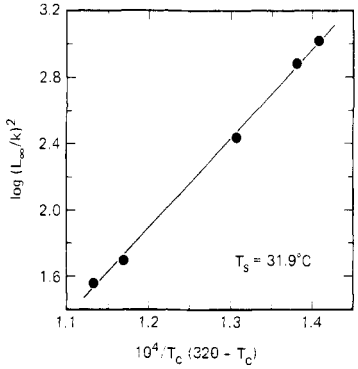


**Figure 11.** Semilogarithmic plot of $(L_\infty/k)^2$, which is proportional to the half-time for crystallization, against $1/T_c(320 - T_c)$.

is a constant for crystals formed in a dilute solution.

To estimate $T_d^0$, the following equation[41] can be used:

$$\frac{1}{T_c} = \frac{1}{T_d^0} + \frac{b}{\Delta H_u}\frac{1}{h_c T_c} \tag{13}$$

where $\Delta H_u$ is the heat of solution per repeat unit and $b$ is a constant that depends on the geometry of the nucleus whose length is here assumed to be the crystal thickness $h_c$. The plot of $1/T_c$ against $1/h_cT_c$ in Figure 10, prepared from the data in Table III, indicates that $T_d^0$ is about 320 K (47 °C), although this value is somewhat uncertain owing to scatter in the values of $h_c$. Values of the long period (LP), also shown in Figure 10, give a $T_d^0$ close to that obtained from the solid line. In analyzing kinetic data for the crystallization of PEO fractions from ethanol, Beech and Booth[9] selected, somewhat arbitrarily, 323 K for $T_d^0$. Also, the data of Kovacs and Manson[7] indicate that $T_d^0$ is about 45 °C for their PS–PEO diblock copolymer in ethylbenzene.

As discussed already, $(L_\infty/k)^2$ is proportional to $t_{1/2}$, the half-time for crystallization. Figure 11 shows that log $(L_\infty/k)^2$ increases linearly with $1/T_c(320 - T_c)$, as predicted by eq 12, the data being those obtained when $T_s$ was 31.9 °C.

From eq 11 and the values of $k$ and $t_0$ in Table II, the time $t^*$ for crystals to attain a size of 1 μm was calculated. Figure 12 shows a semilogarithmic plot of $t^* - t_0$ against the crystallization temperature, no account being taken of the seeding temperature. As indicated in the figure, the slope of the straight-line portion of the curve is 0.26 decade per °C. This slope, though from an empirical representation of the rate data, is similar to that found by Kovacs and Manson[7] for the crystallization of a PS–PEO diblock copolymer from ethylbenzene. They show a semilogarithmic plot of the time for a constant fraction of the crystallization to occur against the crystallization temperature, which was varied from 20 to 30 °C when the

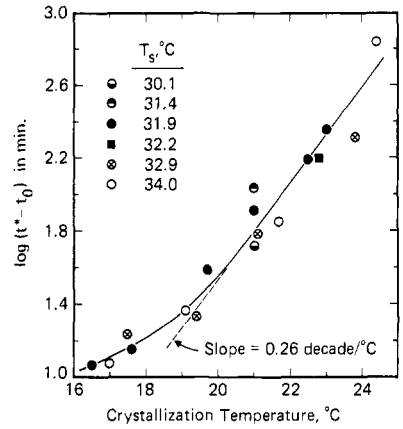


**Figure 12.** Semilogarithmic plot of $t^* - t_0$ against the crystallization temperature, where $t^*$ is the time at which the crystal size is 1 μm, subject to the assumption that eq 11 is valid.

seeding temperature was 35 °C. If their curve, whose curvature is slight, is approximated by a straight line, its slope is 0.24 decade per °C, rather similar to that for the line in Figure 12.

## Summary and Discussion

The present results show that the size of single crystals in a dilute suspension, prepared by the self-seeding method, can be determined accurately and rapidly by measuring the field-free decay of the electric birefringence. The crystals studied were grown in a dilute ethylbenzene solution of a PEO–PPO–PEO triblock copolymer. For certain suspensions of these crystals, the birefringence was found to decay experimentally for values of $\Delta n/\Delta n_0$ between 1 and 0.05, an indication that the crystals were monodisperse. In many instances, however, the decay curve could be represented more accurately by the sum of two exponential terms. This representation gives an average birefringence-relaxation time from which an average crystal size can be obtained. It is given by

$$\langle L^3\rangle^{1/3} = (\sum n_i L_i^5/\sum n_i L_i^2)^{1/3} \tag{14}$$

where again $L_i$ is the length of one side of the $n_i$'th square lamellar crystals.

Such determined values of $\langle L^3\rangle^{1/3}$ for the crystals in three suspensions were found to agree closely with those calculated from the size of 60–100 crystals in each suspension, measured on optical micrographs. The size distribution of the crystals was shown to be quite narrow.

The final size, $L_\infty$, of crystals grown at 21 °C increased from 2.04 to 2.76 μm (Table IV) with an increase in the seeding temperature from 30.1 to 32.9 °C, as expected. However, when the seeding temperature was 31.9 °C, the final size of the crystals increased substantially with a reduction in the crystallization temperature, in qualitative agreement with an unexplained observation reported by Blundell and Keller.[11]

SAXS measurements made on crystals grown after seeding at 34 °C show that the long period increased from 10.7 to 14.6 nm with an increase in the crystallization temperature from 17.2 to 26.0 °C. Measured heats of fusion indicate that the weight fraction of crystalline material in the samples was 0.65 ± 0.03. As the weight fraction of PEO segments in the triblock copolymer is 0.80, the amorphous layer on each side of a crystal contains 19 ± 4% of the units in the PEO segments along with the noncrystallizable PPO segments.

During crystallization, $L$ was found to increase linearly with $t^{1/2}$ until the degree of precipitation was about 0.7. The half-time for crystallization, which is a measure of the

crystallization rate, is proportional to $(L_\infty/k)^2$, where again $k = dL/dt^{1/2}$. Although this observed time dependence is most unusual, it seems that the growth rate of the crystals is controlled by secondary nucleation, as commonly found for homopolymers, because a plot of log $(L_\infty/k)^2$ vs. $1/T_c(320 - T_c)$, prepared from data obtained at five crystallization temperatures $T_c$, gives a straight line of positive slope; i.e., the temperature coefficient of the crystallization rate is negative.

In a study of the growth of crystals from an ethylbenzene solution of a PS–PEO diblock copolymer, Kovacs and Manson[7] found, as already mentioned, that $L$ increases linearly with $t^{1/2}$ over a sizeable portion of the crystallization period. Because the weight fraction of PS in the crystals was less than in the original polymer, they proposed that those molecules containing PS segments significantly longer than the average length were rejected from the growing crystals, thereby causing a progressive reduction in the growth rate with time.

Although the composition of the crystals prepared during our study was not determined, it seems unlikely that fractionation of the PEO–PPO–PEO molecules occurred during crystal growth because the weight fraction of the noncrystallizable PPO segment is half that of the PS segment in the diblock copolymer studied by Kovacs and Manson. Possible support for this statement is provided by the finding[28] that essentially no fractionation occurred during the crystallization from ethylbenzene of a PS–PEO copolymer whose PS content is 28%. (The content of PPO in our copolymer is 20%.) According to the postulate made by Kovacs and Manson, the crystallization kinetics of this latter PS–PEO copolymer should be similar to those of homopolymers. Unfortunately, however, the crystallization kinetics apparently were not determined.

If in fact no fractionation occurred during the crystallization of our PEO–PPO–PEO copolymer, as suggested by the above comments, then a special theoretical treatment is needed to explain the crystallization kinetics of certain block copolymers that contain a noncrystallizable segment.

## References and Notes


(1) Institut für Makromolekulare Chemie, Freiburg, West Germany. Postdoctoral fellow sponsored by IBM, Germany, during 1977–1978.
(2) Holland, V. F.; Lindenmeyer, P. H. *J. Polym. Sci.* **1962**, *57*, 589.
(3) Blundell, D. J.; Keller, A. *J. Polym. Sci., Part B* **1968**, *6*, 433.
(4) Johnsen, U.; Lehmann, J. *Kolloid Z. Z. Polym.* **1969**, *230*, 317, 325.
(5) Keller, A.; Pedemonte, E. *J. Crystal Growth* **1973**, *18*, 111.
(6) Mandelkern, L. *Polymer* **1964**, *5*, 637.
(7) Kovacs, A. J.; Manson, J. A. *Kolloid Z. Z. Polym.* **1966**, *214*, 1.
(8) Devoy, C.; Mandelkern, L.; Bourland, L. *J. Polym. Sci., Part A-2* **1970**, *8*, 869.
(9) Beech, D. R.; Booth, C. *Polymer* **1972**, *13*, 355.
(10) Blundell, D. J.; Keller, A.; Kovacs, A. J. *J. Polym. Sci., Part B* **1966**, *4*, 481.
(11) Blundell, D. J.; Keller, A. *J. Macromol. Sci., Phys.* **1968**, *2*, 301.
(12) Lanceley, H. A.; Sharples, A. *Makromol. Chem.* **1966**, *94*, 30.
(13) Helms, J. B.; Challa, G. *J. Polym. Sci., Part A-2* **1972**, *10*, 761.
(14) Picot, C.; Hornick, C.; Weill, G.; Benoit, H. *J. Polym. Sci., Part C* **1970**, *30*, 349.
(15) Picot, C.; Weill, G. *J. Polym. Sci., Polym. Phys. Ed.* **1974**, *12*, 1733.
(16) Leute, U.; Smith, T. L. *Macromolecules* **1978**, *11*, 707.
(17) Avrami, M. *J. Chem. Phys.* **1939**, *7*, 1103. *Ibid.* **1940**, *8*, 212. *Ibid.* **1941**, *9*, 177.
(18) Booth, C.; Dodgson, D. V. *J. Polym. Sci., Polym. Phys. Ed.* **1973**, *11*, 265.
(19) Fredericq, E.; Houssier, C. "Electric Dichroism and Electric Birefringence"; Clarendon Press: Oxford, 1973.
(20) O'Konski, C. T. *Encycl. Polym. Sci. Technol.* **1968**, *9*, 551.
(21) Stoylov, S. P. *Adv. Colloid Interface Sci.* **1971**, *3*, 45.
(22) O'Konski, C. T.; Krause, S. "Molecular Electro-Optics: Part I—Theory and Methods"; O'Konski, C. T., Ed.; Marcel Dekker: New York, 1976; Chapter 3.
(23) LeFèvre, C. G.; LeFèvre, R. J. W. In "Physical Methods of Organic Chemistry"; Weissberger, A., Ed.; Interscience: New York, 1960; Vol. I, Part III, Chapter 36.
(24) Landolt-Börnstein, Vol. IV, Part 1, p 588.
(25) O'Konski, C. T.; Yoshioka, Y.; Orttung, W. H. *J. Phys. Chem.* **1959**, *63*, 1558.
(26) Yoshioka, K.; Watanabe, H. In "Physical Principles and Techniques of Protein Chemistry"; Leach, S. J., Ed.; Academic Press: New York, 1969; Part A, Chapter 7.
(27) O'Konski, C. T.; Haltner, A. J. *J. Am. Chem. Soc.* **1956**, *78*, 3604.
(28) Lotz, B.; Kovacs, A. J. *Kolloid Z. Z. Polym.* **1966**, *209*, 97.
(29) Lotz, B.; Kovacs, A. J.; Bassett, G. A.; Keller, A. *Kolloid Z. Z. Polym.* **1966**, *209*, 115.
(30) Buckley, C. P.; Kovacs, A. J. *Prog. Colloid Polym. Sci.* **1975**, *58*, 44. *Colloid Polym. Sci.* **1976**, *254*, 695.
(31) Booth, C.; Pickles, C. J. *J. Polym. Sci., Polym. Phys. Ed.* **1973**, *11*, 249.
(32) Beech, D. R.; Booth, C.; Dodgson, D. V.; Sharpe, R. R.; Waring, J. R. S. *Polymer* **1972**, *13*, 73.
(33) Ashman, P. C.; Booth, C. *Polymer* **1975**, *16*, 889.
(34) Kovacs, A. J.; Straupe, C.; Gonthier, A. *J. Polym. Sci., Polym. Symp.* **1977**, *59*, 31.
(35) Price, F. P.; Kilb, R. W. *J. Polym. Sci.* **1962**, *57*, 395.
(36) Simon, F. T.; Rutherford, J. M., Jr. *J. Appl. Phys.* **1964**, *35*, 82.
(37) Booth, C.; Devoy, C. J. *Polymer* **1971**, *12*, 320.
(38) Kloos, F.; Go, S.; Mandelkern, L. *J. Polym. Sci., Polym. Lett. Ed.* **1979**, *17*, 161.
(39) Tadokoro, H. *J. Polym. Sci., Part C* **1966**, *15*, 1.
(40) Hoffman, J. D.; Davis, G. T.; Lauritzen, J. I., Jr. In "Treatise on Solid State Chemistry"; Hannay, N. B., Ed.; Plenum Press: New York, 1976; Vol. 3, pp 497–615. Also: Hoffman, J. D. *SPE Trans.* **1964**, *4*, 315.
(41) Jackson, J. F.; Mandelkern, L. *Macromolecules* **1968**, *1*, 546.